HHS Public Access

Author manuscript

Nat Med. Author manuscript; available in PMC 2010 April 01.

Published in final edited form as:

Nat Med. 2009 October ; 15(10): 1208–1214. doi:10.1038/nm.2019.

Arrested maturation of excitatory synapses in autosomal dominant lateral temporal lobe epilepsy

Yu-Dong Zhou[1], **Sanghoon Lee**[1], **Zhe Jin**[1], **Moriah Wright**[2], **Stephen E. P. Smith**[1], and **Matthew P. Anderson**[1]

[1] Departments of Neurology and Pathology, Harvard Medical School and Beth Israel Deaconess Medical Center, 330 Brookline Ave, E/CLS-717, Boston, MA 02215, USA

[2] Tufts University School of Medicine, 136 Harrison Avenue, Boston, MA 02111, USA

Abstract

A subset of central glutamatergic synapses are coordinatelypruned and matured by unresolved mechanisms during early postnatal life. We report that human epilepsy gene *LGI1*, mutated in autosomal dominant lateral temporal lobe epilepsy (ADLTE), mediates this process in hippocampus. We introduced full-length genes encoding (1) ADLTE truncated mutant LGI1 (835delC) and (2) excess wild-type LGI1 proteins into transgenic mice. We discovered that the normal postnatal Kv1 channel-dependent down-regulation of presynaptic release probability and Src kinase-related decrease of postsynaptic NR2B/NR2A ratio were arrested by ADLTE mutant LGI1, and contrastingly, were magnified by excess wild-type LGI1. Concurrently, mutant LGI1 inhibited dendritic pruning and increased the spine density to markedly increase excitatory transmission. Inhibitory transmission, by contrast, was unaffected. Furthermore, mutant LGI1 promoted epileptiform discharge *in vitro* and kindling epileptogenesis *in vivo* with partial $GABA_A$ receptor blockade. Thus, *LGI1* represents the first human gene mutated to promote epilepsy through impaired glutamatergic circuit maturation.

Many excitatory synapses of the developing vertebrate central nervous system initially overgrow and then are pruned during the third postnatal week1–3. Concurrently, the remaining synapses functionally mature: presynaptic release probability4,5 and postsynaptic NMDA receptor subunit NR2B6 are both down-regulated. In cultured hippocampal neurons, this functional maturation at pre- and postsynaptic sites is synchronous and dependent on integrin and tyrosine phosphorylation 5. Importantly, the molecular pathways and specific neurological disorders linked to this major biological process remain largely undefined.

Correspondence should be addressed To M.P.A. (mpanders@bidmc.harvard.edu). Matthew P. Anderson, M.D., Ph.D., Departments of Neurology and Pathology, Beth Israel Deaconess Medical Center and Harvard Medical School, 330 Brookline Ave, E/CLS-717, Boston, MA 02215, USA.

Note: Supplementary Information is available on the Nature Medicine website.

AUTHOR CONTRIBUTIONS

Y.-D.Z. did electrophysiology, morphological reconstructions, *in vivo* kindling, and EEG recording experiments. S.L. engineered BAC constructs and did characterization. Z.J. and M.W. did immunoblot and genotyping. S.E.P.S. did *in situ* experiment. M.P.A. and Y.-D.Z. designed the study, wrote the paper and were responsible for project planning.

Leucine-rich glioma-inactivated 1 (*LGI1*) was recently discovered to be mutated in human epilepsy disorder ADLTE7–10. ADLTE is characterized by frequent partial seizures (2–5 per month) associated with auditory or other sensory auras during a relatively normal electroencephalogram (EEG). Generalized tonic-clonic seizures occur in the vast majority of patients but are infrequent (~ 1 per year) and may require an environmental trigger. *LGI1* encodes a 64 kDa, secreted, and vertebrate-specific protein that localizes to glutamatergic synapses11–13, binds ADAM22 and ADAM23 (a disintegrin and metalloproteinase domain 22 and 23)13, and co-purifies with pre- and post-synaptic regulatory molecules (presynaptic Kv1.1 potassium channel and postsynaptic density protein PSD95)13,14. Yet, the *in vivo* brain function of LGI1 remains undefined.

A potential role of LGI1 in glutamatergic synapse development was suggested by the finding that LGI1 increases prominently in the brain during the third postnatal week when glutamatergic synapses are pruned and matured (Fig. 1)13. Since LGI1 regulates Kv1.1 channel gating *in vitro*14, both LGI1 and Kv1.1 are strongly expressed at hippocampal medial perforant path-granule cell (MPP-GC) glutamatergic synapses13,14, and GC dendrites re-model during the third postnatal week3, we examined the influence of excess or ADLTE mutant LGI1 protein on postnatal developmental at this major central glutamatergic synapse.

RESULTS

To investigate the functional role of LGI1 in glutamatergic synapse development *in vivo*, we produced two transgenic mouse strains (Supplementary Figs. 1 and 2) using a full-length *LGI1* gene (226 kb, mouse genomic DNA) carried in a bacterial artificial chromosome (BAC) vector15–17. Full-length gene constructs were chosen to preserve native splicing and gene expression patterns so that the effects of altered LGI1 expression on natural brain development could be studied *in vivo*. The first strain was developed with extra copies of the full-length *LGI1* gene to create mice that over-expressed LGI1 protein (LGI1 OE, 64 kDa) (Fig. 1, Supplementary Figs. 1 and 3). The second strain was developed with the same gene as above only engineered with a premature translational stop codon in exon 6, to reproduce the human ADLTE mutation 835delC that truncates the C-terminal epitempin repeat and ADAM22-binding domain (mLGI1, 23 kDa) (Fig. 1, Supplementary Figs. 2 and 3)7. These transgenic constructs were designed, respectively, to magnify *via* LGI1 over expression (~50% increase) and to inhibit *via* dominant negative interference (as reported *in vitro*14) native LGI1 functions. As previously reported *in vitro*11, the quantity of truncated LGI1 protein was low relative to wild-type LGI1 by western blots. We speculate that mLGI1 may fail to secrete and to accumulate at extracellular sites in these transgenic mice *in vivo*.

LGI1 regulates presynaptic function during development

Maturation of presynaptic function (i.e., decrease of release probability) temporally coincided with the expression of LGI1. At p13–p17, when LGI1 expression was weak, paired-pulse facilitation (PPF) of excitatory postsynaptic currents (EPSCs) at MPP-GC synapses was also small (Fig. 1a,b), indicating immature MPP-GC synapses have a high release probability18,19. PPF subsequently increased in mature MPP-GC synapses (Fig.

1a,g) concurrent with the increase of LGI1 (Fig. 1b), indicating LGI1 is expressed when release probability is down-regulated. Since LGI1 co-purifies with Kv1.1 channels, up-regulates Kv1.1 channel currents *in vitro*14, and co-localizes with Kv1.1 channels at MPP-GC synapses14,20, we speculated that release probability may decrease at MPP-GC synapses through LGI1-mediated increases of Kv1.1. Consistent with this notion, Kv1 channel inhibition increases release probability of MPP-GC synapses21,22 and the Kv1 channel-specific blocker α-dendrotoxin (DTX, 100 nM) decreased PPF in mature GCs towards levels observed in immature GCs in wild-type mice (Fig. 1f,g). By contrast, at the lateral perforant path where Kv1.1 is not expressed14,20, DTX had no effect (Supplementary Fig. 4).

To assess whether this developmental down-regulation of MPP release probability is mediated by LGI1, we compared the postnatal change of PPF at MPP-GC synapses in wild-type, mLGI1, and LGI1 OE mice. MPP release probability was similar in all three mouse strains at p13–p17 (Fig. 1a,g), indicating transgenic LGI1 has no effect prior to its expression (Fig. 1b). Importantly, the decrease of MPP release probabilitythat normally occurs in wild-type mice with maturation was blocked in mature mLGI1 mice and magnified in mature LGI1 OE mice (Fig. 1c,g). Furthermore, adding DTX to block Kv1 channels eliminated the difference in MPP release probability found in mature mLGI1 and LGI1 OE mice (Fig. 1f,g). As observed for PPF, other forms of short-term plasticity were also regulated in opposing directions by mutant and excess wild-type LGI1 (Supplementary Fig. 5). This bidirectional regulation of short-term plasticity at MPP-GC synapses firmly establishes a key role for LGI1 in the postnatal regulation of presynaptic function.

LGI1 regulates postsynaptic function during development

A hallmark of postnatal glutamatergic synaptic maturation is the functional change in postsynaptic NR2 subunit composition1,6. To determine whether LGI1 regulates postsynaptic NR2 subunit function at developing MPP-GC synapses, the NMDA receptor subtype-specific antagonists were sequentially added: (R*,S*)-α-(4-hydroxyphenyl)-β-methyl-4-(phenylmethyl)-1-piperidine propanol (Ro 25-6981, 0.5μM, NR2B-specific blocker) and 1-(phenanthrene-2-carbonyl)piperazine-2,3-dicarboxylic acid (PPDA, 5 μM, NR2C/2D blocker) (Fig. 2a). The Ro 25-6981- and PPDA-insensitive current was NR2A-dependent and completelyblocked by 2-amino-5-phosphonovaleric acid (APV, 100 μM, not shown). As PPDA also weakly blocks NR2A/2B-containing NMDA receptors at 5 μM23, the current is denoted NR2A*.

As observed for MPP-GC synapse release probability, the ratio of NR2B to NR2A* current (NR2B/NR2A*) decreased at the approximate time when LGI1 protein increased in wild-type mice (Fig. 2a,b,f). NR2C/D blocker-sensitive currents with a slower inactivation kinetic typical of the NR2D subunit were also observed (Supplementary Table 1)24. Compared to mature wild-type (Fig. 2b,f), the NR2B/NR2A* ratio was larger in mature mLGI1 (Fig. 2c) and smaller in mature LGI1 OE (Fig. 2d). NR2B-containing NMDA receptors are laterally mobile in the membrane25 and are upregulated by Src protein tyrosine kinase26. In addition, tyrosine phosphorylation of synaptosomal proteins decreases around the third postnatal week27 when LGI1 becomes expressed. Therefore, we speculated that LGI1 might down-

regulate NR2B/NR2A ratio by decreasing Src kinase activity. As shown in Supplementary Fig. 6, total Src kinase and phospho-ERK (p-ERK), a substrate activated by Src kinase, were increased in mature mLGI1 mice. Furthermore, Src kinase inhibitor 3-(4-chlorophenyl)1-(1,1-dimethylethyl)-1H-pyrazolo[3,4-d]pyrimidin-4-amine (PP2, 30 min) decreased the NR2B/NR2A* ratio in mature mLGI1 (Fig. 2e,f) and immature wild-type (Fig. 2f) mice compared to their non-treated counterparts. The results suggest LGI1 becomes expressed during the third postnatal week to down-regulate Src kinase and therebydecrease postsynaptic NR2B. In combination, the results establish that LGI1 coordinates the functional maturation of both pre- and post- synaptic properties during postnatal brain development5.

ADLTE mutant LGI1 blocks postnatal dendritic pruning

GC dendrites undergo drastic postnatal remodeling3,28,29. The apical dendrites of GCs grow to become widely and heavily branched during the first two postnatal weeks and are then pruned and narrowed in the third postnatal week3,28, presumably to reduce the complexity of converging entorhinal cortex glutamatergic synaptic inputs. Based on the timing of its expression, we reasoned that LGI1 might also mediate this major structural change during postnatal development.

Immediately before LGI1 was increased, wild-type GCs had a wide and heavily branched apical dendritic arbor (Fig. 3a,f,g) as previously reported3. After LGI1 had increased, the dendritic arbor became narrowed and less branched (Fig. 3b,f,g). Interestingly, Sholl analysis revealed a greater decrease of total dendritic length in the middle molecular layer, where MPP axons form their synapses ($P < 0.01$ in a shell 100 – 170 μm from soma) (Fig. 3e). As predicted, mature mLGI1 GCs displayed a persistently wide and heavily branched apical dendritic arbor typical of immature GCs (Fig. 3c,f,g). Unbalanced two-way ANOVA revealed a significant difference in dendritic length across genetic mouse strains ($F_{3,713} = 6.35$, $P < 0.001$). Tukey\s HSD test further showed that mature mLGI1 GCs had a greater mean dendritic length compared to mature wild-type ($P < 0.05$) and mature LGI1 OE ($P < 0.01$) GCs. The results indicate mLGI1 inhibits postnatal pruning of dendrites.

GCs of the adult mLGI1 mice are not simply immature neurons, since unlike the arrested development of the dendritic arbor, the maturation of passive and active membrane properties occurred normally in mLGI1 GCs (Supplementary Fig. 7)30. Unlike mLGI1, GCs of LGI1 OE mice did not display an immature structure (Fig. 3d–g), but instead developed a shortened apical dendritic arbor (Fig. 3h). The latter result suggests excess LGI1 may promote excessive pruning of dendrites.

Mutant LGI1 not only inhibited apical dendrite branch pruning, but also doubled apical dendrite spine density (Fig. 3i,j). Interestingly, LGI1 OE did not affect spine density, suggesting possible compensatory preservation (Fig. 3i,j). In conclusion, LGI1 expression during postnatal development not only coordinates the maturation of pre- and postsynaptic function, but also remodels apical dendrite branches and spines.

ADLTE mutant LGI1 increases excitatory synaptic transmission

The finding that ADLTE mutant LGI1 arrests the functional maturation and the structural trimming of glutamatergic synapses suggested mLGI1 might enhance excitatory transmission. Consistent with this prediction, the amplitude of evoked AMPA and NMDA receptor-mediated EPSCs (Fig. 4a–d) and the frequency of miniature EPSCs (mEPSCs) (Fig. 4e,f) were increased in mature mLGI1 compared to wild-type. By contrast, these properties were reduced in mature LGI1 OE (Fig. 4a–f). The amplitude of mEPSCs was only modestly increased by mLGI1 and unaffected by LGI1 OE (right panel in Fig. 4f), suggesting only minor effects on AMPA receptor density at synapses. To compare excitatorytransmission in the absence of the differences in presynaptic release probability, we added Kv1 channel blocker DTX (100 nM). In DTX, maximum EPSC amplitude was approximately doubled in mLGI1 and unaffected in LGI1 OE mice compared to wild-type (Fig. 4g). These functional changes closely parallel the structural doubling of spine density observed in mLGI1 and the absence of LGI1 OE effect. Together the results suggest mLGI1 increases total glutamatergic synapse number.

The balance of excitatory and inhibitory synaptic currents is critical in determining the efficacy of synaptic transmission. To directly compare glutamatergic and GABAergic synapses on a cell-by-cell basis, spontaneous EPSCs and IPSCs (sEPSCs and sIPSCs) were recorded by alternately clamping at AMPA or $GABA_A$ receptor channel reversal potential31. This strategy revealed that sEPSC charge transfer was increased (Fig. 5a,b) while sIPSC charge transfer was unaltered (Fig. 5a,c) in mLGI1, causing an increased sEPSC/sIPSC charge transfer ratio (Fig. 5d). Furthermore, directly stimulating middle molecular layer GABAergic fibers with glutamatergic synapses blocked evoked IPSCs of similar amplitude in each strain ($F_{2,81} = 2.7$, $P > 0.05$) (Fig. 5e,f). Finally, miniature IPSC (mIPSC) amplitude (Fig. 5g,h) and interevent interval (Fig. 5g,i) did not differ across strains. The results indicate LGI1 selectively regulates the glutamatergic synapse in dentate granule neurons.

ADLTE mutant LGI1 increases seizure susceptibility

To assess for pathophysiological consequences of enhanced excitatory synaptic transmission in mLGI1, we examined seizure susceptibility *in vitro* and *in vivo*. Generalized seizure incidence is low in ADLTE and 5 d of EEG recording failed to reveal spontaneous seizures in mLGI1 mice (Anderson, unpublished data). In mLGI1 mice, although excitatory transmission was increased, total inhibitory transmission still vastlyexceeded excitatory transmission. This may explain the incomplete penetrance in carriers and the predominance of partial seizures in individuals with ADLTE. The increased excitatory transmission, however, predicts a lowered seizure threshold with partial GABAergic transmission blockade. Stimulating MPP induced a field excitatory postsynaptic potential (fEPSP) in the GC layer (Fig. 6a–c)32 and at most a single population spike (Fig. 6a–c,e). Adding low dose picrotoxin (PTX, 50μM) increased the number and the maximum peak-to-peak amplitude of population spikes in all three strains (Fig. 6a–c,e,f)33. However, in mLGI1, the spike number exceeded wild-type and LGI1 OE (Fig. 6e). Similarly, PTX increased the normalized maximum peak-to-peak amplitude of population spikes to a greater extent in mLGI1 than in wild-type mice ($P < 0.05$, Fig. 6f). Furthermore, afterdischarges33, a marker

of recurrent activity, occurred in four of five PTX-treated hippocampal slices of mLGI1 (Fig. 6d), but never in wild-type or LGI1 OE.

The enhanced epileptiform discharge of mLGI1 brain slices *in vitro* suggested the possibility of increased seizure susceptibility with $GABA_A$ receptor blockade *in vivo*. Repeated intraperitoneal injections of subconvulsive doses of $GABA_A$ receptor antagonist pentylenetetrazol (PTZ, 30 mg/kg) every other day, a model of kindling epileptogenesis, leads to a progressively lower seizure threshold and provides a robust and reproducible measure of seizure susceptibility. As seizure kindling progressed, four types of aberrant EEG patterns were successively observed and were used to score seizure intensity (Supplementary Figs. 8 and 9)34. Initial paroxysmal EEG events were rhythmic spikes, spike-and-waves, or polyspike-and-waves that occurred in 0.5–3 s bursts (Supplementary Fig. 9a). Fully kindled mice displayed a decrescendo spike-and-wave EEG pattern typical of clonic seizures. The pre-convulsive paroxysmal EEG events were identifiable by their abrupt onset and offset and progressive increase of 4–7 Hz power (Supplementary Fig. 9c). Normalized theta band power was proportional to EEG pattern score, progressively increasing during kindling. Using these measures, mLGI1 mice were shown to develop clonic seizures much earlier than their wild-type littermates (Fig. 6j–l). After the 6^{th} PTZ injection, seven of eight mLGI1, but only two of eight wild-type, mice responded with a clonic seizure (representative trace shown in Fig. 6g). The EEG pattern of LGI1 OE and wild-type littermate mice was dominated by spike-and-wave EEG patterns on the 6^{th} PTZ injection (Fig. 6h,i). Normalized theta band power confirmed that mLGI1 mice develop clonic seizures earlier than LGI1 OE and control mice (hippocampus: $F_{3,276} = 7.26$, $P \ll 0.05$; cortex: $F_{3,276} = 4.71$, $P < 0.05$) (Fig. 6k,l). Behavioural measures of the seizure response to repeated subconvulsive PTZ injections in a separate cohort showed similar results (Supplementary Fig. 10). Interestingly, once mice were fully kindled, the latency and duration of clonic seizures did not differ across strains (Supplementary Fig. 11). The results indicate ADLTE mLGI1 promotes kindling epileptogenesis.

DISCUSSION

These results define the major function of the gene mutated to cause human ADLTE and uncover a key molecular agent regulating postnatal glutamatergic synapse development. LGI1 regulated the functional maturation and structural pruning of glutamatergic synapses during postnatal development (Supplementary Fig. 12). LGI4, another family member, plays a similar postnatal role in developmental myelination of peripheral nerves35. ADLTE mutant LGI1 arrested the development of hippocampal MPP-GC excitatory synapses, causing a drastic increase of excitatory transmission. As the dentate gyrus gates seizure propagation through hippocampus36,37, the findings could have direct relevance to human seizure dissemination. Indeed mice carrying mLGI1 were prone to kindling epileptogenesis.

Our results suggest LGI1 acts at the presynaptic terminal to overcome Kvβ1-mediated Kv1.1 channel inhibition *in vivo* during postnatal development. Kv1 channel blocker DTX eliminated the differences caused by the *LGI1* transgenes on presynaptic release probability (Fig. 2), suggesting LGI1 reduces presynaptic release probability by up-regulating presynaptic Kv1 potassium channels *in vivo*. The result is consistent with *in vitro* studies

showing LGI1 antagonizes Kvβ1-promoted Kv1.1 channel inactivation14. Significantly, Kv1.1 is already expressed at the adult level during the third postnatal week38, and Kvβ1 is developmentally up-regulated during this same time period (Anderson, unpublished data). Directly measuring Kv1.1 channels function at the minute MPP synaptic terminus is currently not technically feasible, but future studies aimed at larger synapses that express LGI1 will be important.

Postsynaptic NMDA receptor trafficking is of particular importance to synapse maturation and plasticity39. Our results indicate that Src kinase activity plays a critical role in maintaining the high level of NR2B-containing NMDA receptor function present at MPP-GC synapses during early postnatal development (Fig. 3). Interestingly, both LGI1 and integrin5 seem to coordinate the developmental maturation of pre- and postsynaptic function of glutamatergic synapses. Furthermore, both LGI1 and integrin bind the same disintegrin domain of the ADAM family proteins13,40 and regulate NR2 subunit composition *via* tyrosine kinase signaling (Fig. 3)5. In future studies, it will be important to determine whether LGI1 and integrin interact *via* ADAM family members to promote glutamatergic synapse maturation and pruning.

In contrast to our results, exogenous application of LGI protein to hippocampal brain slices failed to affect release probability at Schaffer collateral-CA1 pyramidal cell synapses in p24–p29 rodents13. Our results indicate release probability is already fully down-regulated by the high levels of native LGI1 present by p24–p29. Furthermore, ADAM22 is only weakly expressed in the Schaffer collateral (www.neuromab.org/datasheet/N46_30.pdf). Exogenous LGI1 was also reported to produce a small increase of the AMPA/NMDA ratio, mEPSC amplitude, and mEPSC frequency13. By contrast, our transgenic mice with excess LGI1 displayed a decreased mEPSC frequency and no change in mEPSC amplitude. Differences in the amount, distribution, or target of exogenous vs. endogenous LGI1 may explain these differing results.

Our results indicate LGI1 acts to remodel the hippocampal dentate glutamatergic circuitry. Dendritic arbor pruning may remove excess excitatory connections formed during early development. Although the detailed cellular mechanisms remain unknown, interactions between LGI1 and the postsynaptic cellular scaffolding molecule PSD95 might be important41.

LGI1 did not regulate GABAergic synaptic functions measured in dentate gyrus, but inhibitory exceeded excitatory transmission by approximately 20-fold (Fig. 5a). This observation suggests the strong inhibition might mask the increased excitatory transmission caused by mLGI142. Future studies should evaluate whether LGI1 regulates glutamatergic synapses onto GABAergic neurons as these could also partially compensate for the pro-epileptic effects of mLGI1.

The opposing effects of mLGI1 and excess full-length LGI1 indicate mLGI1 acts as a dominant negative inhibitor to cause epilepsy14, rather than through haploid insufficiency7,11. The dominant negative mechanism remains undefined, but could result from hetero-multimer formation between mLGI1 and wild-type LGI1 *via* cysteine residues

within the N-terminal leucine-rich repeat domain13. Since the dominant negative effects of mLGI1 occurred in the critical period of postnatal development, we suggest ADLTE mLGI1 may disrupt normal brain development in early childhood to promote epilepsy throughout adulthood.

METHODS

All protocols were approved by BIDMC Institutional Animal Care and Use Committee.

Generation of LGI1 transgenic mice

We generated HA-tagged full-length LGI1 and mutant LGI1 (835delC) BAC (RP23-121N12) constructs following PCR-based methods in combination with the lambda red recombinase system (Supplementary Figs. 1 and 2)15–17. The 226 kb mouse LGI1 BAC contains the entire 41 kb *LGI1* genomic locus, plus 163 kb 5′ flanking and 21 kb 3′ flanking genomic regions. We prepared BAC DNA using double acetate precipitation and $CsCl_2$ gradient purification methods. We linearized BAC DNA using restriction enzyme PI-Sce (NEB) and microinjected BAC DNA in the BIDMC transgenic core facility.

Electrophysiological recording

We prepared brain slices of hippocampus from C57BL mice (mean age (in d): immature, 15.3 ± 0.4, n = 20; mature WT, 93.7 ± 10.2, *n* = 39; mLGI1, 97.7 ± 10.8, *n* = 26; LGI1 OE, 98.7 ± 11.9, *n* = 21). We anaesthetized adult mice with 2,2,2-tribromoethanol (0.25 mg/g) and transcardially perfused them with ice-cold sucrose-containing saline. We cut 280 μm transverse slices of hippocampus with a cut made through the hilus to limit the mossy fiber influence. We performed whole-cell recordings of dentate granule cells at a temperature of 35–36 °C. We evoked excitatory synaptic currents by MPP stimulation with a saline-filled glass electrode placed 200 μm away from the recording site. We recorded AMPA receptor-mediated synaptic currents at −80 mV. We carried out paired-pulse facilitation experiments to estimate the release probability. We recorded NMDA receptor-mediated synaptic currents at a holding potential of +40 mV using a cesium-based internal solution in the presence of 10 μM DNQX, 100 μM picrotoxin, and 20 μM glycine. We recorded spontaneous EPSCs and IPSCs at −60 mV and +10 mV, respectively, using the cesium-based internal solution and a low divalent ion ACSF. We recorded miniature EPSCs at −60 mV using the cesium-based internal fluid and regular saline containing 0.5 μM TTX and 50 μM picrotoxin. We recorded miniature IPSCs at +10 mV using the cesium-based internal fluid and regular ACSF containing 0.5 μM TTX, 10 μM DNQX, and 50 μM APV. We elicited field excitatory synaptic potential (fEPSP) by stimulating the MPP and recording with a regular ACSF-filled patch pipette placed in the GC layer 200 μm from the stimulating electrode. See Supplementary Methods online for more details.

Histochemistry

We used the intracellular solution containing 0.5% biocytin to fill GCs. We fixed brain slices of hippocampus with biocytin-filled GCs in 4% para-formaldehyde in PBS for 24 h. We performed standard avidin-biotinylated horseradish peroxidase staining (ABC-Elite kit, Invitrogen). We mounted the developed slices with Mowiol. We reconstructed detailed

morphology of GCs using a Nikon microscope equipped with an ApoPlan 100x/1.4 oil immersion objective under the control of Neurolucida software (MicroBrightField).

In-situ hybridization

See Supplementary Methods online for more details.

Western blot

We used 10 % SDS-PAGE to separate the proteins. After transferring the gels to nitrocellulose membranes, we incubated the membranes in a variety of primary antibodies (LGI1, 1:250, Santa Cruz; β-actin, 1:250, Cell Signalling; Src, 1:1000, Cell Signalling; ADAM22, 1:1000, NeuroMab; PSD95, 1:1000, NeuroMab). The membranes were then incubated with horseradish peroxidase-conjugated secondary antibody (1:10,000) and developed using either ECL or ECL-Plus Western blotting detection reagents.

PTZ kindling

See Supplementary Methods online for more details.

Intracranial EEG recording and analysis

We made intracranial electrodes from polyimide insulated stainless steel wire with a bare diameter of 0.2 mm (Plastics One). We implanted three wires onto the skull of two-month old mice according to the stereotaxic coordinates of the recording site targets (in mm): Bregma −2.3, lateral 1.7, and depth 2.0 for the hippocampal area; Bregma −0.8, lateral 1.8, and depth 1.3 for the contralateral parietal cortex; and Bregma −3.8, lateral 1.8, and depth 1.5 for the reference electrode43. We buffered and recorded local field potentials with a Neuralynx preamplifier (HS-27, Neuralynx) and amplified (gain: 2000), band-filtered (0.1–2000 Hz), and digitized (sampling rate: 5 kHz) with a Neuralynx Cheetah system (Neuralynx). We wrote Custom Matlab (MathWorks) scripts to extract 3 s segments from the original EEG recordings with their power spectral density normalized to baseline theta frequency power (4–7 Hz) (Supplementary Fig. 8). We identified four distinct aberrant EEG patterns associated with PTZ injections (Supplementary Fig. 9)34. We scored aberrant EEG events: 0, normal EEG pattern; 1, rhythmic spikes; 2, spike-and-waves; 3, polyspike-and-waves; 4, decrescendo spike-and-waves. The final EEG score of an EEG recording represents the highest scored aberrant EEG event occurring in this recording session.

Statistics

We reported data as means ± s.e.m. We performed two-tailed unpaired Student’s t-test and Kolmogorov-Smirnov test to compare group means and cumulative distributions, respectively. We used unbalanced two-way ANOVA and post-ANOVA Tukey’s honestly significant difference (HSD) test to compare group variance.

Supplementary Material

Refer to Web version on PubMed Central for supplementary material.

Acknowledgments

We would like to thank C. B. Saper, J. S. Flier, D. K. Simon, G. D. Rosen, M. R. Kasten, and M. W. Anderson for comments and suggestions, and G. D. Rosen for help on the Neurolucida system. This work was supported in part by the US National Institute of Neurological Disorders and Stroke R01 NS057444-01A2 (M.P.A.), the Nancy Lurie Marks Family Foundation (M.P.A.), Autism Speaks/NAAR (M.P.A.), and Beth Israel Deaconess Medical Center.

References

1. Waites CL, Craig AM, Garner CC. Mechanisms of vertebrate synaptogenesis. Annu Rev Neurosci. 2005; 28:251–274. [PubMed: 16022596]
2. Chen C, Regehr WG. Developmental remodeling of the retinogeniculate synapse. Neuron. 2000; 28:955–966. [PubMed: 11163279]
3. Rihn LL, Claiborne BJ. Dendritic growth and regression in rat dentate granule cells during late postnatal development. Brain Res Dev Brain Res. 1990; 54:115–124. [PubMed: 2364540]
4. Bolshakov VY, Siegelbaum SA. Regulation of hippocampal transmitter release during development and long-term potentiation. Science. 1995; 269:1730–1734. [PubMed: 7569903]
5. Chavis P, Westbrook G. Integrins mediate functional pre- and postsynaptic maturation at a hippocampal synapse. Nature. 2001; 411:317–321. [PubMed: 11357135]
6. Barth AL, Malenka RC. NMDAR EPSC kinetics do not regulate the critical period for LTP at thalamocortical synapses. Nat Neurosci. 2001; 4:235–236. [PubMed: 11224537]
7. Kalachikov S, et al. Mutations in LGI1 cause autosomal-dominant partial epilepsy with auditory features. Nat Genet. 2002; 30:335–341. [PubMed: 11810107]
8. Morante-Redolat JM, et al. Mutations in the LGI1/Epitempin gene on 10q24 cause autosomal dominant lateral temporal epilepsy. Hum Mol Genet. 2002; 11:1119–1128. [PubMed: 11978770]
9. Ottman R, et al. LGI1 mutations in autosomal dominant partial epilepsy with auditory features. Neurology. 2004; 62:1120–1126. [PubMed: 15079011]
10. Steinlein OK. Genetic mechanisms that underlie epilepsy. Nat Rev Neurosci. 2004; 5:400–408. [PubMed: 15100722]
11. Senechal KR, Thaller C, Noebels JL. ADPEAF mutations reduce levels of secreted LGI1, a putative tumor suppressor protein linked to epilepsy. Hum Mol Genet. 2005; 14:1613–1620. [PubMed: 15857855]
12. Sirerol-Piquer MS, et al. The epilepsy gene LGI1 encodes a secreted glycoprotein that binds to the cell surface. Hum Mol Genet. 2006; 15:3436–3445. [PubMed: 17067999]
13. Fukata Y, et al. Epilepsy-related ligand/receptor complex LGI1 and ADAM22 regulate synaptic transmission. Science. 2006; 313:1792–1795. [PubMed: 16990550]
14. Schulte U, et al. The epilepsy-linked Lgi1 protein assembles into presynaptic Kv1 channels and inhibits inactivation by Kvβ1. Neuron. 2006; 49:697–706. [PubMed: 16504945]
15. Datsenko KA, Wanner BL. One-step inactivation of chromosomal genes in Escherichia coli K-12 using PCR products. Proc Natl Acad Sci USA. 2000; 97:6640–6645. [PubMed: 10829079]
16. Anderson MP, et al. Thalamic Cav3.1 T-type Ca^{2+} channel plays a crucial role in stabilizing sleep. Proc Natl Acad Sci USA. 2005; 102:1743–1748. [PubMed: 15677322]
17. Uzzau S, Figueroa-Bossi N, Rubino S, Bossi L. Epitope tagging of chromosomal genes in Salmonella. Proc Natl Acad Sci USA. 2001; 98:15264–15269. [PubMed: 11742086]
18. Min MY, Asztely F, Kokaia M, Kullmann DM. Long-term potentiation and dual-component quantal signaling in the dentate gyrus. Proc Natl Acad Sci USA. 1998; 95:4702–4707. [PubMed: 9539802]
19. Thomson AM. Facilitation, augmentation and potentiation at central synapses. Trends Neurosci. 2000; 23:305–312. [PubMed: 10856940]
20. Monaghan MM, Trimmer JS, Rhodes KJ. Experimental localization of Kv1 family voltage-gated K^+ channel alpha and beta subunits in rat hippocampal formation. J Neurosci. 2001; 21:5973–5983. [PubMed: 11487620]

21. Meiri N, Sun MK, Segal Z, Alkon DL. Memory and long-term potentiation (LTP) dissociated: normal spatial memory despite CA1 LTP elimination with Kv1.4 antisense. Proc Natl Acad Sci USA. 1998; 95:15037–15042. [PubMed: 9844011]
22. Meiri N, et al. Reversible antisense inhibition of Shaker-like Kv1.1 potassium channel expression impairs associative memory in mouse and rat. Proc Natl Acad Sci USA. 1997; 94:4430–4434. [PubMed: 9114006]
23. Lozovaya NA, et al. Extrasynaptic NR2B and NR2D subunits of NMDA receptors shape 'superslow' afterburst EPSC in rat hippocampus. J Physiol. 2004; 558:451–463. [PubMed: 15146049]
24. Thompson CL, Drewery DL, Atkins HD, Stephenson FA, Chazot PL. Immunohistochemical localization of N-methyl-D-aspartate receptor subunits in the adult murine hippocampal formation: evidence for a unique role of the NR2D subunit. Brain Res Mol Brain Res. 2002; 102:55–61. [PubMed: 12191494]
25. Tovar KR, Westbrook GL. The incorporation of NMDA receptors with a distinct subunit composition at nascent hippocampal synapses in vitro. J Neurosci. 1999; 19:4180–4188. [PubMed: 10234045]
26. Prybylowski K, et al. The synaptic localization of NR2B-containing NMDA receptors is controlled by interactions with PDZ proteins and AP-2. Neuron. 2005; 47:845–857. [PubMed: 16157279]
27. Cudmore SB, Gurd JW. Postnatal age and protein tyrosine phosphorylation at synapses in the developing rat brain. J Neurochem. 1991; 57:1240–1248. [PubMed: 1895104]
28. Rahimi O, Claiborne BJ. Morphological development and maturation of granule neuron dendrites in the rat dentate gyrus. Prog Brain Res. 2007; 163:167–181. [PubMed: 17765718]
29. Ge S, et al. GABA regulates synaptic integration of newly generated neurons in the adult brain. Nature. 2006; 439:589–593. [PubMed: 16341203]
30. Liu YB, Lio PA, Pasternak JF, Trommer BL. Developmental changes in membrane properties and postsynaptic currents of granule cells in rat dentate gyrus. J Neurophysiol. 1996; 76:1074–1088. [PubMed: 8871221]
31. Dani VS, et al. Reduced cortical activity due to a shift in the balance between excitation and inhibition in a mouse model of Rett syndrome. Proc Natl Acad Sci USA. 2005; 102:12560–12565. [PubMed: 16116096]
32. Patel LS, Wenzel HJ, Schwartzkroin PA. Physiological and morphological characterization of dentate granule cells in the p35 knock-out mouse hippocampus: evidence for an epileptic circuit. J Neurosci. 2004; 24:9005–9014. [PubMed: 15483119]
33. Buckmaster PS, Dudek FE. Network properties of the dentate gyrus in epileptic rats with hilar neuron loss and granule cell axon reorganization. J Neurophysiol. 1997; 77:2685–2696. [PubMed: 9163384]
34. Velišek, L. Models of chemically-induced acute seizures. In: Pitkänen, A.; Schwartzkroin, PA.; Moshé, SL., editors. Models of Seizures and Epilepsy. Academic Press; 2005. p. 127-152.
35. Bermingham JR Jr, et al. The claw paw mutation reveals a role for Lgi4 in peripheral nerve development. Nat Neurosci. 2006; 9:76–84. [PubMed: 16341215]
36. Brenner R, et al. BK channel β4 subunit reduces dentate gyrus excitability and protects against temporal lobe seizures. Nat Neurosci. 2005; 8:1752–1759. [PubMed: 16261134]
37. Hsu D. The dentate gyrus as a filter or gate: a look back and a look ahead. Prog Brain Res. 2007; 163:601–613. [PubMed: 17765740]
38. Grosse G, et al. Expression of Kv1 potassium channels in mouse hippocampal primary cultures: development and activity-dependent regulation. J Neurosci. 2000; 20:1869–1882. [PubMed: 10684888]
39. Lau CG, Zukin RS. NMDA receptor trafficking in synaptic plasticity and neuropsychiatric disorders. Nat Rev Neurosci. 2007; 8:413–426. [PubMed: 17514195]
40. Yang P, Baker KA, Hagg T. The ADAMs family: coordinators of nervous system development, plasticity and repair. Prog Neurobiol. 2006; 79:73–94. [PubMed: 16824663]
41. Charych EI, et al. Activity-independent regulation of dendrite patterning by postsynaptic density protein PSD-95. J Neurosci. 2006; 26:10164–10176. [PubMed: 17021172]

42. Coulter DA, Carlson GC. Functional regulation of the dentate gyrus by GABA-mediated inhibition. Prog Brain Res. 2007; 163:235–243. [PubMed: 17765722]

43. Wu C, Wais M, Sheppy E, del Campo M, Zhang L. A glue-based, screw-free method for implantation of intra-cranial electrodes in young mice. J Neurosci Methods. 2008; 171:126–131. [PubMed: 18420280]

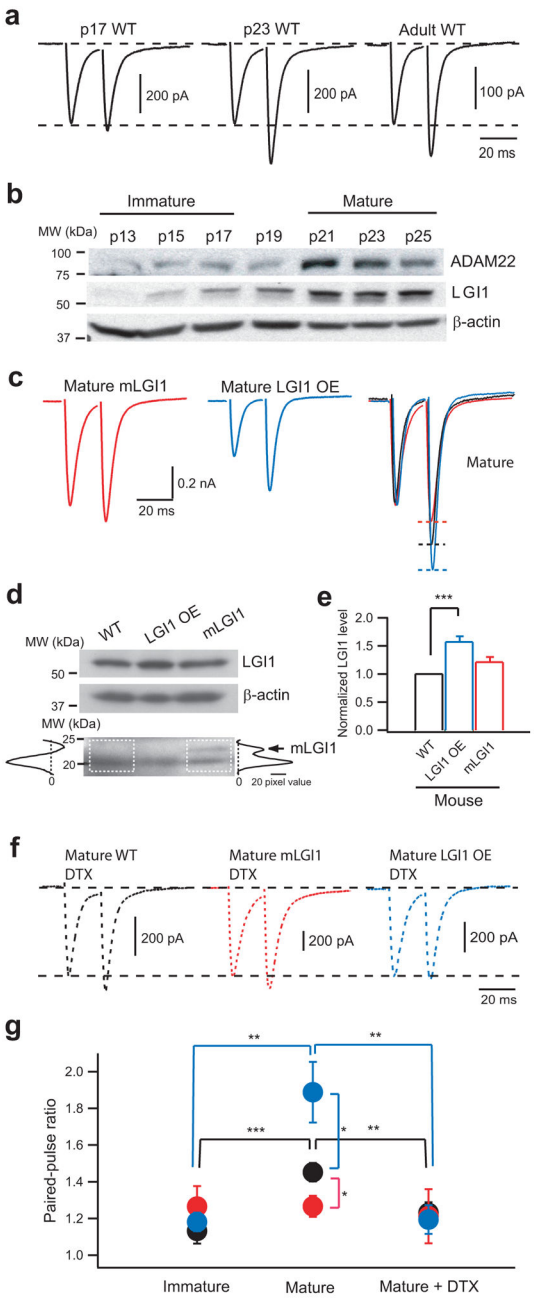

Figure 1.

LGI1 down-regulates presynaptic release probability at hippocampal MPP-GC excitatory synapses *via* Kv1 channels during postnatal development. (**a**) Representative traces showing paired-pulse facilitation (PPF) of evoked MPP-GC postsynaptic currents, a measure of release probability, increases between postnatal days 17 and 23 in control (WT) mice. (**b**) Western blots showing LGI1 and its receptor, ADAM22, also increase between p17 and p23. (**c**) Representative traces showing PPF remains low in mature mLGI1 and significantly increases in mature LGI1 OE mice relative to control. (**d**) Western blot showing increased expression of 64 kDa LGI1 in LGI1 OE mice and expression of 23 kDa mutant LGI1,

marked by an arrow on densitometry traces, in mLGI1 mice. (**e**) Quantification of 64 kDa LGI1 protein density (normalized to β-actin) in WT, LGI1 OE, and mLGI1 mice (n = 7). (**f**) Kv1 channel blocker α-dendrotoxin (DTX) eliminates the difference in paired-pulse ratio (ppr) in mature mice. (**g**) Quantification of ppr in WT (black symbols), mLGI1 (red symbols), and LGI1 OE (blue symbols) mice (n = 4 to 25). *: $P < 0.05$; **: $P < 0.01$; ***: $P < 0.001$.

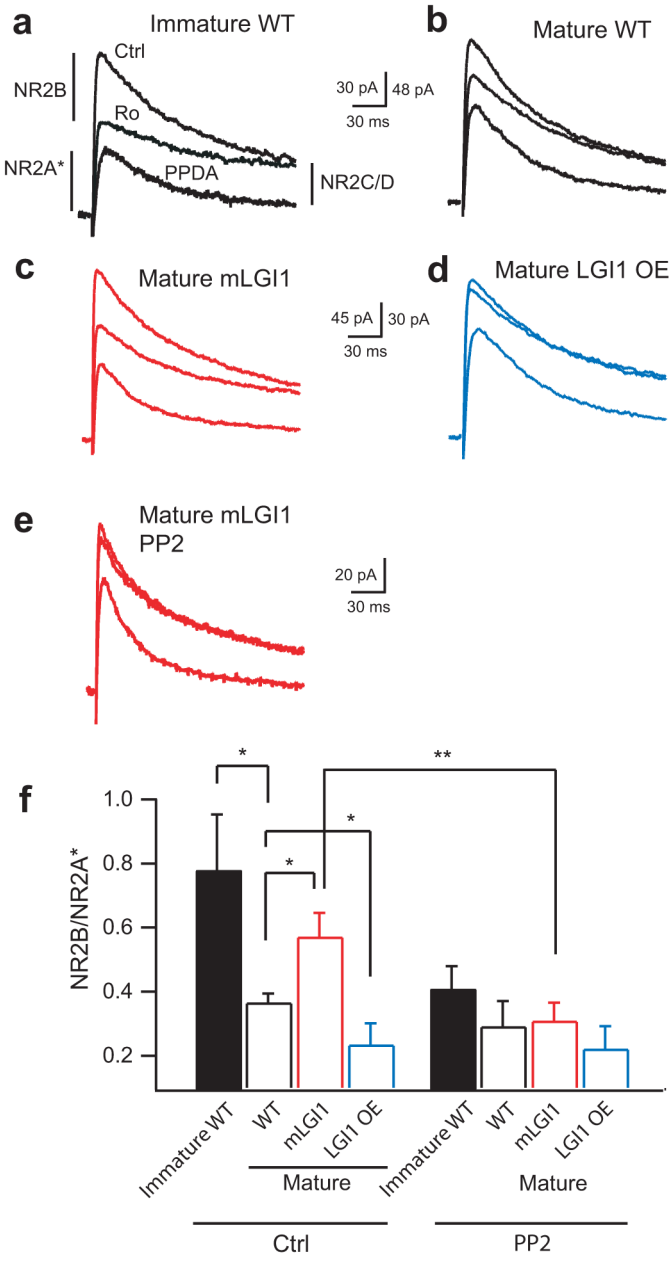

Figure 2.

LGI1 down-regulates postsynaptic NR2B-dependent NMDA receptor currents during postnatal brain development. (**a,b**) Representative current traces from wild-type (WT) showing NR2B subunit-dependent current is larger in immature (**a**) than mature (**b**) wild-type GCs. Ro: NR2B blocker; PPDA: NR2C/2D blocker. (**c,d**) Representative current traces showing NR2B-dependent currents remain high in mature mLGI1 (**c**) and down-regulate excessively in mature LGI1 OE (**d**) transgenic mice relative to mature wild-type (**b**). (**e**) Representative traces showing Src kinase inhibitor, PP2, inhibits the NR2B component in mature mLGI1. (**f**) Quantification of NR2B/NR2A* current ratio in the three genotypes (*n* =

5 to 11) across postnatal development in the presence and absence of PP2. *: $P < 0.05$; **: $P < 0.01$.

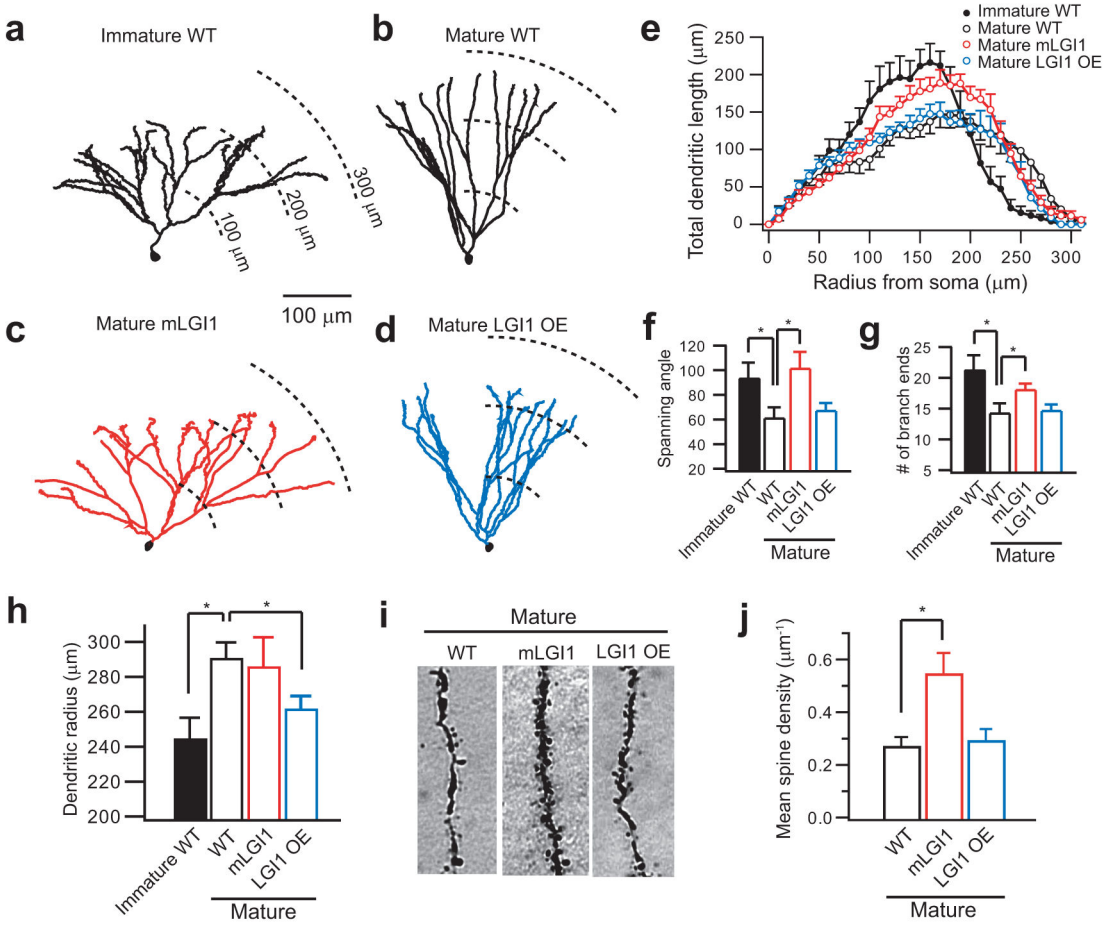

Figure 3.

ADLTE mutant LGI1 blocks dendritic pruning during postnatal development and increases spine density. (**a,b**) Representative Neurolucida-reconstructed wild-type (WT) GC dendrites showing a widely branched arbor in immature GCs (**a**) and a less branched arbor in mature GCs (**b**). (**c,d**) Representative Neurolucida-reconstructed GC dendrites showing a widely branched arbor in mature mLGI1 GCs (**c**) and a shortened arbor in mature LGI1 OE GCs (**d**). (**e**) Sholl analysis of GC dendritic arbor. (**f–h**) Quantification of dendritic spanning angle (**f**), branch end number (**g**), and mean radius (**h**) of immature WT (*n* = 7), mature WT (n = 6), mature mLGI1 (*n* = 7), and mature LGI1 OE (*n* = 7) GCs. (**i,j**) Representative images (**i**) and quantification of mean spine density(**j**) showing an increased spine number in mature mLGI1 GCs (*n* = 4) compared to mature WT (*n* = 5) and mature LGI1 OE (*n* = 6) GCs. *: $P < 0.05$.

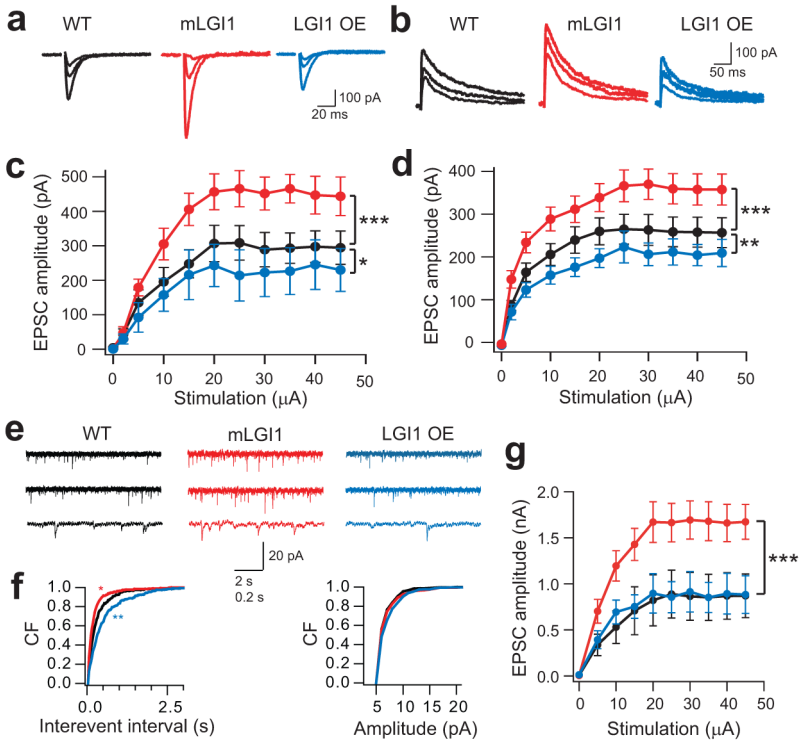

Figure 4.

ADLTE mutant LGI1 increases glutamatergic synaptic transmission. (**a,b**) Representative traces showing evoked AMPA (**a**) and NMDA (**b**) receptor-mediated EPSCs (2 μA, 5 μA, and saturating stimulus intensities) in wild-type (WT), mLGI1, and LGI1 OE mice. (**c,d**) Quantification of EPSC amplitude to stimulus intensity for AMPA (**c,** WT, black, *n* = 10; mLGI1, red, *n* = 7; LGI1 OE, blue, *n* = 6) and NMDA (**d,** WT, black, *n* = 11; mLGI1, red, *n* = 11; LGI1 OE, blue, *n* = 7) receptor currents. (**e**) Representative traces showing mEPSCs recorded from GCs of WT, mLGI1, and LGI1 OE transgenic mice. (**f**) Cumulative frequency plots of mEPSC interevent interval and amplitude for WT (black), mLGI1 (red), and LGI1 OE (blue) transgenic mice (*n* = 5). (**g**) Quantification of maximum evoked EPSC in DTX in WT (black symbol, *n* = 3), mLGI1 (red symbol, *n* = 4), and LGI1 OE (blue symbol, *n* = 3) mice. *:$P < 0.05$; **: $P < 0.01$; ***: $P < 0.001$.

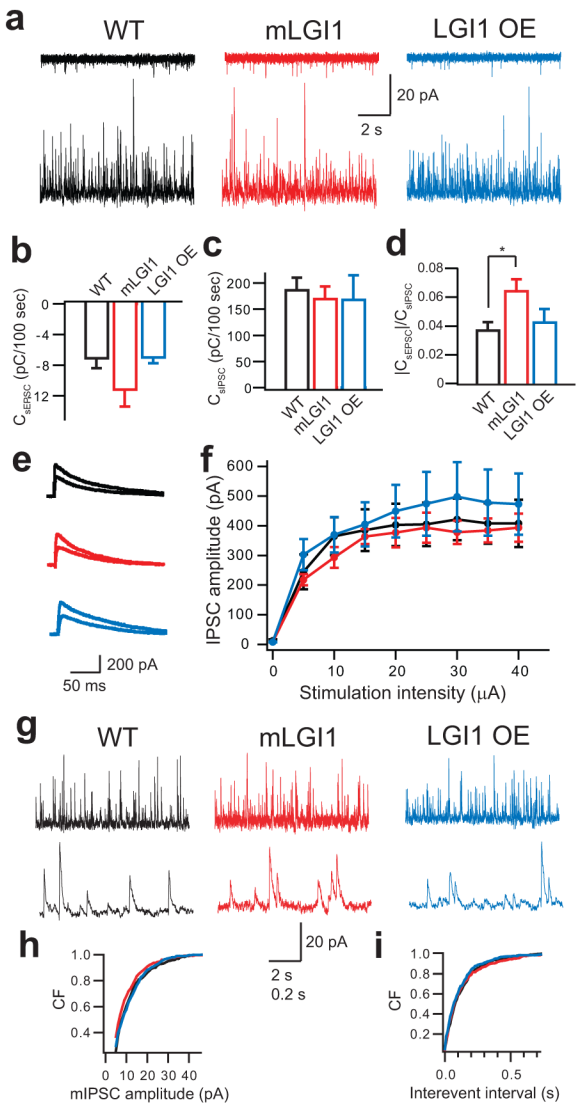

Figure 5.

LGI1 trangenes fail to effect inhibitory synaptic transmission. **(a)** Representative traces showing spontaneous EPSC (sEPSC, upper) and IPSC (sIPSC, lower) recorded in the same cell at –60 mV (upper) and +10 mV (lower) from wild-type (WT, black), mLGI1 (red), and LGI1 OE (blue) transgenic mice. (**b–d**) Quantification of sEPSC (**b**) and sIPSC (**c**) charge transfer and sEPSC/sIPSC charge transfer ratios (**d**) in WT (n = 10), mLGI1 (n = 9), and LGI1 OE (n = 4) mice. (**e**) Representative traces showing evoked $GABA_A$ receptor-mediated IPSC (5 μA, and saturating stimulus intensities) in WT (black), mLGI1 (red), and LGI1 OE (blue) mice. (**f**) Quantification of evoked IPSC amplitudes for WT (black), mLGI1 (red), and LGI1 OE (blue) mice (n = 4). (**g**) Representative traces showing miniature IPSC (mIPSC) recorded from GCs of wild-type, mLGI1, and LGI1 OE mouse. (**h,i**) Cumulative frequency plots of mIPSC amplitude (**h**) and interevent interval (**i**) for WT (black), mLGI1 (red), and LGI1 OE (blue) (n = 5). *: $P < 0.05$.

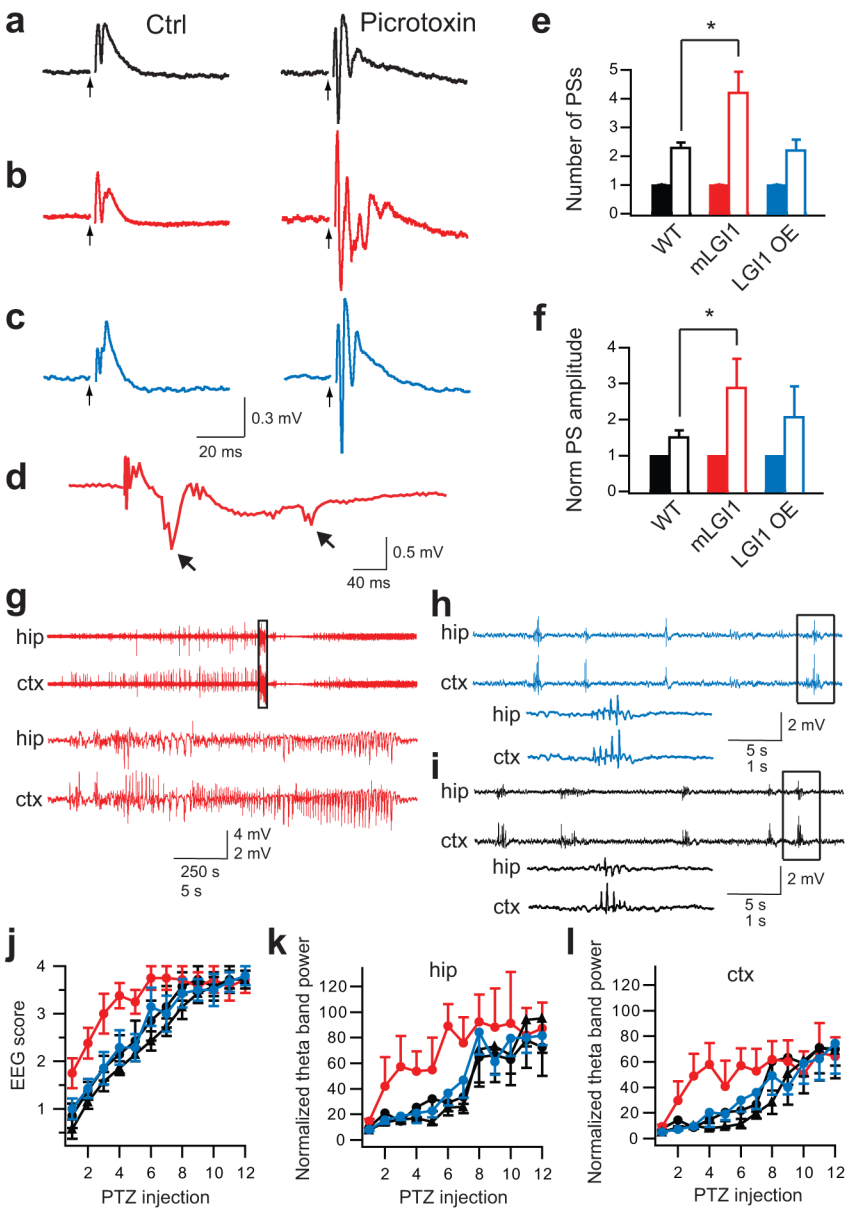

Figure 6.

ADLTE mutant LGI1 promotes epilepsy. (**a–c**) Representative traces showing field potentials from the GC layer of wild-type (WT) (**a**), mLGI1 (**b**), and LGI1 OE (**c**) mice in response to MPP stimulation (arrow heads) before (left) and after (right) picrotoxin (PTX) treatment. (**d**) Representative trace showing afterdischarges (arrows) followed population spikes only in PTX-treated mLGI1 slices. (**e,f**) Quantification of mean population spike (PS) number (**e**) and normalized maximum amplitude (**f**) for WT (black) (*n* = 7), mLGI1 (red) (*n* = 5), and LGI1 OE (blue) (*n* = 6) mice before (solid bars) and after (open bars) PTX treatment. (**g–i**) Representative EEG traces from mLGI1 (**g**), LGI1 OE (**h**), and WT littermate (**i**) mice after 6th PTZ injection. The areas marked by the rectangles are expanded in the lower traces. (**j–l**) Quantifications of EEG scores (**j**), normalized hippocampal (**k**), and

cortical (**l**) EEG theta band power of PTZ-kindling in mLGI1 mice (red circles) (n = 8) vs. their wild-type littermates (black circles) (n = 8), and LGI1 OE mice (blue circle) (n = 7) vs. their wild-type littermates (black triangles) (n = 7). *: $P < 0.05$.